# Quantitative Imaging of Molecular Order in Lipid Membranes Using Two-Photon Fluorescence Polarimetry

Alicja Gasecka,[†] Tsai-Jung Han,[†] Cyril Favard,[†] Bong Rae Cho,[‡] and Sophie Brasselet[†]*
[†]Institut Fresnel-MOSAIC Group, UMR 6133, Centre National de la Recherche Scientifique, Université Aix Marseille III, Domaine Universitaire St Jerome, Marseille, France; and [‡]Molecular Optoelectronics Laboratory and Department of Chemistry, Korea University, Seoul, Korea

ABSTRACT We present a polarimetric two-photon microscopy technique to quantitatively image the local static molecular orientational behavior in lipid and cell membranes. This approach, based on a tunable excitation polarization state complemented by a polarized readout, is easily implementable and does not require hypotheses on the molecular angular distribution such as its mean orientation, which is a main limitation in traditional fluorescence anisotropy measurements. The method is applied to the investigation of the molecular angular distribution in giant unilamellar vesicles formed by liquid-ordered and liquid-disordered micro-domains, and in COS-7 cell membranes. The highest order contrast between ordered and disordered domains is obtained for dyes locating within the membrane acyl chains.

## INTRODUCTION

Molecular order is a key parameter in a large variety of biological phenomena. Measuring orientational information is essential for understanding of the molecular interactions that drive the morphology of biomolecular assemblies, from membrane protein aggregates to biopolymers involved in signaling events, cell mechanics, and adhesion. Imaging such organizations quantitatively using optical microscopy remains a challenge. Essentially, this issue has been approached by fluorescence anisotropy measurements from molecular probes localized at adequate and functional positions. This technique is based on a ratiometric analysis on two states of incident and analyzed polarizations, resulting in two accessible parameters $I_{//}$ and $I_{\perp}$ depending on the parallel or perpendicular configuration of the incident versus analyzed directions. However, so far, investigations on non-isotropic samples have been limited (1–9). Fluorescence anisotropy is only successful in cases restricted to cylindrical symmetry geometries of the molecular angular distributions, and necessitates an a priori knowledge of either the mean orientation of the molecular distribution, or its shape (10). It also contains redundancies such as the impossibility of differentiating the cases of an isotropic distribution from that of a 45° (relative to the // or $\perp$ directions) molecular orientation. This obviously limits the possible range of applications of this method, since most biomolecular interactions occur in complex structures of unknown symmetry axes.

We propose here to use a polarimetric approach where multiple polarization states are analyzed. Recent works in polarization-resolved, second-harmonic generation microscopy have demonstrated that rich information is contained in polarization responses recorded from a tunable-incident linear polarization in the sample plane (11)—for instance, to distinguish, specifically, the local nature (symmetry, disorder) of molecular assemblies in molecular monolayers (12) and in crystals down to the nanometer scale (13,14). In this work, we implement a polarimetric two-photon excitation fluorescence (TPEF) imaging technique, based on the polarized readout of the fluorescence response to a tunable incident polarization state. Two-photon excitation is chosen for its intrinsic advantages relative to one photon fluorescence: in addition to less scattering, deeper optical penetration, and intrinsic spatial resolution (typically 300-nm lateral), the nonlinear nature of the excitation indeed reduces the angular photoselection and thus ameliorates the angular sensitivity of polarized measurements. We show that polarimetric TPEF circumvents the weaknesses of fluorescence anisotropy imaging by providing information on molecular order without any hypothesis on the average orientation of the molecules. This technique is applied to the investigation of the local molecular organization in heterogeneous artificial membranes and in cell membranes. Giant unilamellar vesicles (GUVs) made of lipid mixtures, which are considered as model systems for the investigation of lipid interactions (15–18), exhibit coexisting domains with different fluidity, elasticity, and polarity properties. This phase segregation into gel, liquid-ordered, and -disordered environments, is closely related to fundamental cell processes, particularly for cell signaling, where the existence of lipid-specific functional rafts platforms is still a debate (19–25). So far, imaging lipid domains has relied on the use of dedicated fluorescent probes specifically partitioning in regions of known lipid composition or local polarity (26–28). Such probes are also expected to undergo specific orientational orders detectable by fluorescence anisotropy (26,27,29). However, so far, no direct imaging of molecular order in heterogeneous lipid domains has been attempted. Here we illustrate the application of TPEF polarimetry on two issues that cannot be addressed by a pure ratiometric method: the

*Submitted February 18, 2009, and accepted for publication August 28, 2009.*

*Correspondence: sophie.brasselet@fresnel.fr

Editor: Lukas K. Tamm.



0006-3495/09/11/2854/9 $2.00

doi: 10.1016/j.bpj.2009.08.052

investigation of the orientational organization in coexisting liquid phase with short-range order (Lo) and disordered liquid (Ld) fluid domains of micrometric sizes in GUVs, and in cell membranes of nonspherical shapes. The studied GUVs are formed from a ternary mixture of the lipids sphingomyelin, 1,2-dioleoyl-*sn*-glycero-3-phosphocholine (DOPC), and cholesterol (15). Lo domains are known to be essentially constituted by enriched sphingomyelin and cholesterol regions, whereas DOPC is mainly present in disordered liquid regions. The labeling of the lipid mixtures is performed using different fluorescent probes present in both types of domains: 6-dodecanoyl-2-dimethylamine-naphthalene (Laurdan) (26), 6-dodecanoyl-2-[*n*-methyl-*n*-(carboxymethyl)amino]naphthalene (C-Laurdan) (27), 1-(4-trimethyl ammonium-phenyl)-6-phenyl-1,3,5-hexatriene (TMA-DPH), and di-8-ANEPPQ. Laurdan and C-Laurdan are specifically chosen for their ability to provide a spectral identification (and thus a control measurement) of the Lo and Ld domains location on a GUV. A quantity of 1,1′-dioctadecyl-3,3,3′,3′-tetra methyl indo carbocyanine perchlorate (DiI-$C_{18}$) is also used as a preliminary control for the Lo and Ld domains identification (28).

We show that polarimetric measurements permit a quantitative analysis of the local molecular order in different phases of the GUVs and in cell membranes, independently of the position investigated on the vesicle or cell contour. We introduce, in the data analysis, the effects of distinct absorption and emission angles of the molecular transition dipoles, as well as the presence of fluorescence resonance energy transfer (homo-FRET) in the membrane.

## MATERIALS AND METHODS

### Materials

The fluorescent lipid probes TMA-DPH, $DiIC_{18}$, di-8-ANEPPQ, and Laurdan were purchased from Invitrogen Molecular Probes (Carlsbad, CA). C-Laurdan was synthesized by the group of Bong Rae Cho from Korea University in Seoul, South Korea (27). DOPC and cholesterol (Chol) were obtained from Avanti Polar Lipids, and chicken egg yolk sphingomyelin (SM) from Sigma Aldrich (St. Louis, MO). Lipids were used without further purification and were stored in chloroform/methanol (9:1) at −20°C until use.

### GUVs and cell lines sample preparation

The giant unilamellar vesicles (GUVs) were prepared according to the electroformation method developed by Angelova and Dimitrov (30). First, 10 μL of a 6.6 mM solution of DOPC, cholesterol, and SM (1:1:1) loaded with fluorescent lipid probes (1:1000) were deposited at 40°C on two glass slides covered with indium tin oxide. This temperature is chosen to facilitate the evaporation of chloroform. The chloroform elimination was completed by drying the slides under vacuum for 1 h. The slides were then sealed together and solvent (428 mM solution of sucrose in water) was added to the chamber and heated to the desired temperature (above the lipid mixture phase transition, 55°C for DOPC/cholesterol/SM). In the last step, the chamber was connected to an electrical generator (AC Exact, model No. 128; Exact Electronics, Hillsboro, OR). An 8 Hz, 25 mV peak-to-peak sinusoidal voltage was applied. It was increased by 100 mV steps every 5 min, up to a value of 1225 mV. These conditions were maintained overnight. Next, the application of electrical square pulses of the same amplitude at 4 Hz detached the GUVs from the slides. With this approach, we have obtained GUVs with diameter ranging from 10 to 80 μm.

COS-7 cells (No. CRL-1657; American Type Culture Collection, Manassas, VA) were maintained in 37°C with DMEM medium (Lonza Braine, Brussels, Belgium) completed by 5% fetal bovine serum, and penicillin-streptomycin (50 units/mL). Before measurement, cells were transferred onto glass coverslips, incubated for 3.5 h, washed twice with insertion buffer (NaCl 130 mM, KCl 5 mM, CaCl 210 mM, glucose 5 mM, and HEPES 10 mM (pH 7.4)) and then stained with 5 μM di-8-ANEPPQ (dissolved by absolute ethanol to 1 mM for preservation and usage) for 5 min. The cells were then washed twice again and kept at room temperature in the insertion buffer for the whole imaging process. TPEF polarimetry on cell membranes was performed at room temperature.

### Experimental setup

The experimental setup used in TPEF microscopy is depicted in the Supporting Material (Fig. S1). The excitation light source is a tunable Ti:Sapphire laser (Chameleon, Coherent, Santa Clara, CA) that delivers 150-fs pulses at a repetition rate 80 MHz. The incident wavelength is set at 780 nm for C-Laurdan, Laurdan, TMA-DPH, and di-8-ANEPPQ, and 1040 nm for $DiIC_{18}$, with a typical averaged power of a few mWs. The laser beam is reflected by a dichroic mirror and focused on the sample by a high numerical aperture objective (water immersion objective, ×60, 1.2 numerical aperture (NA); Nikon, Melville, NY). The backward-emitted signal is collected by the same objective and directed to a polarization beamsplitter that separates the beam toward two avalanche photodiodes (model No. SPCM-AQR-14; PerkinElmer, Boston, MA) used in photon-counting mode. Images are performed by the scanning of the sample on a piezoelectric stage, which allows precise location of polarimetric measurement points. The TPEF polarimetric measurement consists in continuously rotating the linear polarization of the incident laser beam in the sample plane by an achromatic half waveplate mounted on a step rotation motor at the entrance of the microscope. For each value of the polarization angle, the emitted signal is recorded on the two perpendicular directions *X* and *Y* defining the sample plane. These directions also correspond to the *s* and *p* reflection directions for the dichroic beamsplitter. A polarimetric image stack of 90 polarization angles is typically recorded within a few minutes, which can be lowered down to a few seconds by decreasing the angular resolution.

### Theory

Modeling two-photon excited fluorescence (TPEF) processes in molecular media necessitates accounting for molecular two-photon absorption and one-photon emission properties, their statistical orientational distribution, and finally the incident and analyzed field polarization states. The molecular angular distribution of fluorescent lipid probes is defined here by a normalized molecular orientational probability distribution function $f(\theta, \phi)$, with $(\theta, \phi)$ as the spherical angles denoting the molecular frame orientation (Fig. 1 *a*). The value $f(\theta, \phi)$ is related to the potential energy $U(\theta, \phi)$ of the molecule, according to the Boltzmann equilibrium relation $f(\theta, \phi) \propto \exp(-U(\theta, \phi)/k_BT)$. In lipid membranes, the orientational distribution is most often defined as a cone shape (1,2,31), with an abrupt change of the probe potential at a defined aperture angle $\theta = v$. In this case, $f(\theta, \phi) = 1/(4\pi v)$ for $\theta \leq v$ and $f(\theta, \phi) = 0$ otherwise. Different functions could be equally introduced such as a cone contour $f(\theta, \phi) = \delta(\theta - v)$ (5) or a normalized Gaussian distribution $f(\theta, \phi) = (\sqrt{\ln 2}/v)\exp(-\ln 2\theta^2/v^2)$ (4). The most general distribution function is a decomposition over spherical harmonics with orders of symmetry *J*, which weights can be independently retrieved up to $J = 6$ using polarization-resolved TPEF (14). In lipid membranes $f(\theta, \phi)$ is expected to be a $\theta$-dependent cylindrical symmetry function, which can be restricted to the order parameters $\langle P_{J=2,4,6}\rangle$ defined as $\langle P_J\rangle = \int f(\theta)P_J(\cos\theta)\sin\theta d\theta$ (with $P_J(\cos\theta)$ the *J*-order Legendre polynomials) (2,4,31).

The orientation of the angular distribution function in the macroscopic frame is defined by the orientation angle $(\rho, \eta)$ of its symmetry axis, as

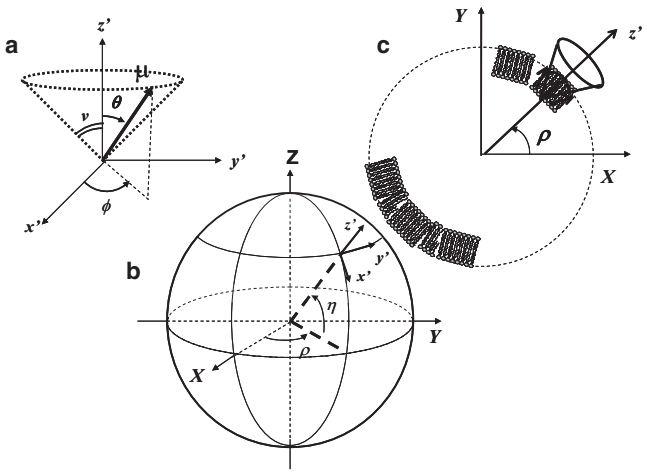


FIGURE 1 Definition of the coordinates used in the analysis. (*a*) In the microscopic frame, the *v*-parameter is the cone aperture of the distribution function. The values ($\theta$, $\phi$) define the orientation of the molecular dipole in the cone frame. (*b*) In the laboratory frame, the *Z* axis is the optical axis, and *X* and *Y* denote the sample plane in which the excitation polarization is defined. The angles $\rho$ and $\eta$ specify the cone orientation in the macroscopic frame. (*c*) Experimental configuration. The excitation light is focused on an equatorial point of the GUV where $\eta = 0$.

illustrated in Fig. 1, *a* and *b*, in the case of a cone distribution. Note that this orientation does not necessarily correspond to the membrane-normal direction. Fig. 1 *c*, which illustrates the case where the distribution axis coincides with the membrane normal in a spherical GUV or cell, shows the experimental configuration where light is focused on an equatorial point ($\eta = 0$). In this situation the relevant parameters of the molecular distribution are $v$ and $\rho$. The TPEF response from one molecule depends on

1. the relative orientations of the excitation dipole and the incident field and
2. the emission dipole orientation.

The first development assumes that the excitation and emission dipoles are parallel, the case of different orientations being more extensively described below. The orientation of the excitation/emission dipole is given by the respective polar and azimuthal angles $\theta$ and $\sigma$ in the membrane frame ($x'$, $y'$, $z'$), as described in Fig. 1 *a*. The components of the excitation dipole moment in the laboratory frame (*X*, *Y*, *Z*) are given by

$$\begin{bmatrix}\mu_X(\theta,\phi,\rho,\eta)\\ \mu_Y(\theta,\phi,\rho,\eta)\\ \mu_Z(\theta,\phi,\rho,\eta)\end{bmatrix} = \begin{bmatrix}-\sin\rho & -\cos\rho\sin\eta & \cos\rho\cos\eta\\ \cos\rho & -\sin\rho\sin\eta & \sin\rho\cos\eta\\ 0 & \cos\eta & \sin\eta\end{bmatrix}\cdot\begin{bmatrix}\sin\theta\cos\phi\\ \sin\theta\sin\phi\\ \cos\theta\end{bmatrix}. \quad (1)$$

The TPEF signal from one single molecule is proportional to the product of two-photon excitation and one-photon emission probabilities (11). The emission contribution originates from the radiation of the molecule emission dipole integrated over the broad range of collection angles by the high NA objective. This effect is taken into account in the emission contribution intensities $J_X$ and $J_Y$ from the single dipole $\vec{\mu}(\theta,\phi,\rho,\eta)$ and measured after the objective for two respective *X* and *Y* orthogonal states of analysis directions, following (1)

$$\begin{aligned} J_X(\theta,\ \phi,\ \rho,\ \eta) &= K_1\mu_X^2(\theta,\ \phi,\ \rho,\ \eta) + K_2\mu_Y^2(\theta,\ \phi,\ \rho,\ \eta) + K_3\mu_Z^2(\theta,\ \phi,\ \rho,\ \eta),\\ J_Y(\theta,\ \phi,\ \rho,\ \eta) &= K_2\mu_X^2(\theta,\ \phi,\ \rho,\ \eta) + K_1\mu_Y^2(\theta,\ \phi,\ \rho,\ \eta) + K_3\mu_Z^2(\theta,\ \phi,\ \rho,\ \eta), \end{aligned} \quad (2)$$

where the coefficients $K_1$, $K_2$, and $K_3$ quantify the mixing among the contributions of different polarization components into the final fluorescence intensity. In the present case of an NA = 1.2 objective, $K_1 = 0.86$, $K_2 = 0.015$, and $K_3 = 0.262$ (1).

The single molecule two-photon excitation probability is proportional to $|\vec{\mu}\cdot\vec{E}|^4$, with $\vec{\mu}$ the absorption dipole and $\vec{E}$ the incident optical field. The time-averaged fluorescence intensity of an ensemble of molecules within an orientational distribution $f(\theta,\phi)$, analyzed along a given polarization state $i = (X, Y)$, can finally be expressed as the incoherent sum over individual fluorescent intensities (11)

$$I_i(\rho,\eta,\alpha,v) = \int_0^{2\pi}\int_0^{\pi} |\vec{\mu}_i(\theta,\phi,\rho,\eta)\cdot\vec{E}(\alpha)|^4 J_i(\theta,\phi,\rho,\eta) \times f(\theta,\phi)\sin\theta d\theta d\phi, \quad (3)$$

when $\vec{E}(\alpha)$ is a linear polarization state vector oriented with an angle $\alpha$ relative to *X*. In the polarimetric measurement developed in this work, $\alpha$ is a tunable parameter varying from 0° to 360°, obtained by rotating a half-wave plate at the entrance of the microscope. The TPEF polarization responses along the *X* and *Y* analysis directions are defined as the fluorescence intensities measured along the two detectors (Fig. S1). The main difference with fluorescence anisotropy is that in our case, the whole range of incident polarization angles is exploited. Here a complete analysis of the molecular orientational distribution is therefore possible, using $\rho$, $\eta$, and $v$ as fitting parameters. Any other distribution could be investigated using other representative fitting parameters or general order parameters.

In Eq. 3, $\vec{E}(\alpha)$ has to be defined at the focal point of the objective. Due to the epi-geometry of the imaging setup, the input polarization undergoes a reflection on the dichroic beamsplitter, which affects its linear state, by adding ellipticity and dichroism at intermediate $\alpha$-angles (11,32). The phase difference $\delta$ between the *X* and *Y* components of the field (ellipticity) and their amplitude factor (dichroism $\gamma$) are determined separately, using a calibration procedure previously described (32); this gives $\delta = 0.26$ and $\gamma = 0.005$ for the dichroic beamsplitter used in this work.

## RESULTS

For all experiments and simulations, the polarization responses are represented as polar diagrams where each measurement points is a vector pointing from the origin, with an amplitude equal to the fluorescence intensity, and a tilt angle relative to *X* equal to $\alpha$. This allows a direct visualization of the fluorescence angle dependence, relative to a rotation of the excitation field polarization.

### Influence of $\rho$, $v$, $\eta$, and the angular distribution shape on the polarimetric responses

The theoretical TPEF polarization responses $I_X(\alpha)$ and $I_Y(\alpha)$ emitted by an assembly of fluorescent molecules are depicted in Fig. 2 for different distribution parameters $v$ and $\rho$, assuming $\eta = 0$ and a cone-shape angular distribution. For relatively small aperture angles ($v < \pi/6$), the molecules exhibit a quasi one-dimensional order and thus very

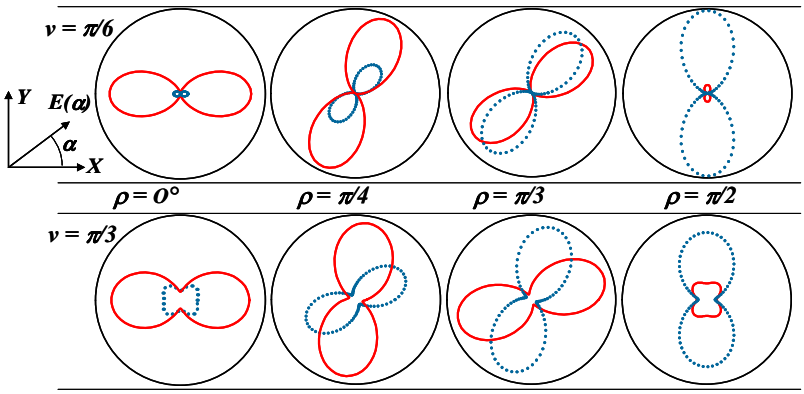


FIGURE 2 Influence of the $\rho$- and $v$-parameters on polar polarization plots representing the calculated TPEF intensities $I_X$ (*solid line*) and $I_Y$ (*dotted line*) as functions of the incident field rotation angle $\alpha$. The polar plots description is given in the text. The *X* and *Y* sample plane macroscopic axes indicated here are identical in all the following polar plots figures. The dichroic parameters $\delta = 0.26$ and $\gamma = 0.005$ are used in this model for the incident field polarization state, which is representative of the experimental configuration.

anisotropic $I_X$ and $I_Y$ polarization responses. For larger cone apertures, these two lobes are strongly deformed, due to the contribution of a broader range of dipole orientations. Fig. 2 shows that this polarimetric analysis is strongly sensitive to both width and mean orientation of the angular distribution of the molecules: whereas the mean orientation $\rho$ is seen to predominantly affect the overall pointing direction of the polarization lobes responses, the cone aperture $v$ affects the relative deformation of these lobes. This approach shows that measurements with high angular accuracy can be obtained with no a priori knowledge of either $\rho$- or $v$-values.

The effect of the out-of-plane orientation angle $\eta$ of the cone aperture shows that for $\eta$-angles below 45°, the polarimetric responses are seen to be essentially independent on $\eta$ (only minor deviations being seen in the curves amplitude). According to the experimental geometry, the measured distributions are located on the equatorial perimeter of the membranes; therefore $\eta$ is expected to lie close to 0° in this study.

At last, TPEF polarimetric responses significantly depend on the molecular angular distribution shape, which makes it a possible probe for angular orientational behaviors. Fig. 3 depicts $I_X$ and $I_Y$ polarization responses for three different $f(\theta, \phi)$ distributions described above: cone, Gaussian, and cone-contour. The three functions have a full width at half-maximum equal to $v$. Although of similar dependence with a two-lobe shape response, the cone and Gaussian models exhibit some differences in the opening of the lobes. The cone-contour model is very different and can be easily discriminated from filled-apertures models, which is not the case in traditional fluorescence anisotropy measurements (5).

## Determination of $v$ in two-phase lipid mixtures GUVs

The polarimetric TPEF technique is applied to the investigation of the static orientational order of different fluorescent probes in GUVs lipid membranes made of Lo and Ld phases obtained from DOPC/Chol/SM mixtures. Fluorescent probes sensitive to their lipid phase environment are first used to validate the use of polarimetric measurements: at 780-nm excitation, C-Laurdan and Laurdan in raft mixtures made

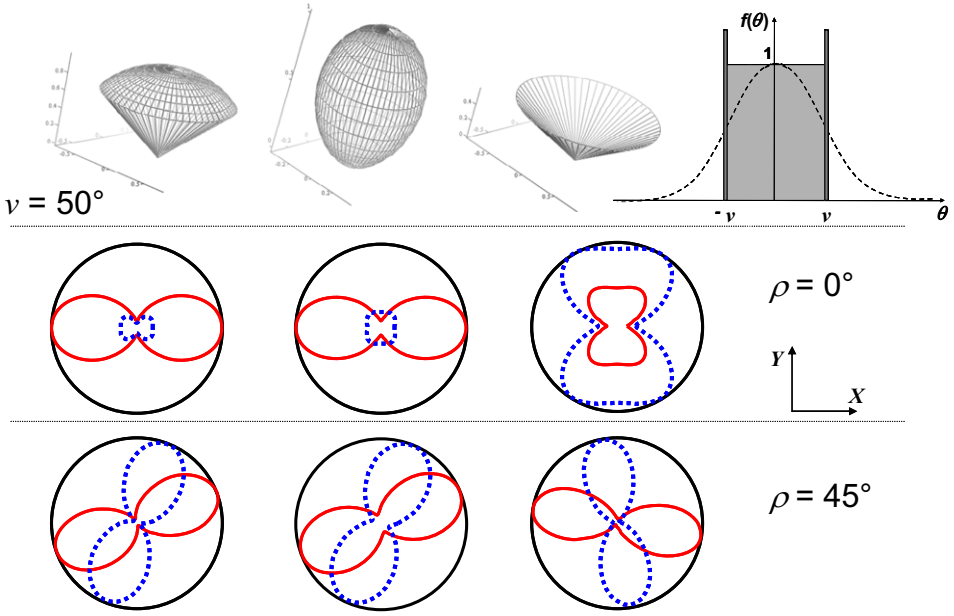


FIGURE 3 Two-photon polarimetric responses $I_X$ (*solid line*) and $I_Y$ (*dotted line*) as a function of the incident field rotation angle $\alpha$ for different angular distributions of the fluorescent molecules at fixed $\rho = 0, 45°$ and $v = 50°$ parameters. (From *left* to *right*) Cone, Gaussian, and cone-contour distributions, all of them have a full width at half-maximum equal to $v$ as represented on their $\theta$-dependent section (far right graphic). The dichroic parameters $\delta = 0.26$ and $\gamma = 0.005$ are used in this model.

of both Lo and Ld phases are known to exhibit broad emission spectra with two maxima. The first one, at ~440 nm, reflects the Lo phase whereas the second one, at ~490 nm, is attributed to the Ld phase. By using appropriate filters, the location of the two phases in a GUV can be discriminated. The presence of both domains is furthermore ascertained by colocalization measurements using DiI-$C_{18}$ as an additional probe, which is known to locate in Ld domains in such lipid mixtures (28). All further analyzes are done without the DiI-$C_{18}$ fluorophore in the membranes.

TPEF polarimetric responses of C-Laurdan and Laurdan in DOPC/Chol/SM GUVs are depicted in Fig. 4, *a* and *b*, for different points on the GUVs. In this experiment, no specific spectral filtering is used; therefore, the lipid domains are not distinguishable in the image. The fitting of the polarimetric responses is performed for both intensities $I_Y$ and $I_X$, on both parameters $v$ and $\rho$, using the angular distribution models described above. The mean orientation angle of the distribution $\rho$ is therefore not artificially introduced, but is deduced from the data fitting. In addition for a given position on the GUV, $v$ can be determined with a $\pm 0.5^\circ$ precision, with a slight increase of this error margin to $\pm 2^\circ$ at high cone apertures (in this situation, the shape of the polarization responses is less sensitive to the $\rho$-orientation, as can be expected from a large angular distribution of molecules).

Firstly, the data are seen to be consistent with models close to a cone or a Gaussian aperture. The cone-contour model can be discarded since it leads to very different polarimetric dependencies (Fig. 3). A thorough analysis of the fitting accuracy shows that a Gaussian model seems more adapted than a cone shape to the observed phenomenon (Fig. S2). This is consistent with a statistically driven orientational behavior, measured at equilibrium. From the fitting of the polarimetric angular dependencies, both cone and Gaussian models lead to similar $\rho$- and $v$-values.

Secondly, the deduced mean orientation $\rho$ of the molecular distribution is seen to also correspond to the measured normal direction of the membrane in the studied location.

At last, the measured distribution aperture angles $v$ can be clearly discriminated in two populations associated with high and low aperture angles (Fig. 4 *c*). By comparing the spatial location of the observed populations on the GUVs using a spectral filtering imaging (Fig. 4 *d*), we deduce that these two populations can be assigned to the Lo and Ld lipid environments. The obtained $v$ values are summarized in Table 1, together with the corresponding order parameters $\langle P_{J=2,4,6} \rangle$ defined above. The Lo phase is overall characterized by a lower distribution aperture than in the Ld phase, and by higher $\langle P_{J=4,6} \rangle$ order parameters (the high $J$ orders are indeed signatures of a narrow angular distribution).

A similar study was performed for the TMA-DPH and di-8-ANEPPQ fluorescent probes, which do not significantly modify their spectral emission behavior in Ld and Lo phases. The TPEF polarimetric responses for these probes in DOPC/Chol/SM GUVs are depicted in Fig. 5, *a* and *b*. The fits obtained from different points of the GUVs clearly show

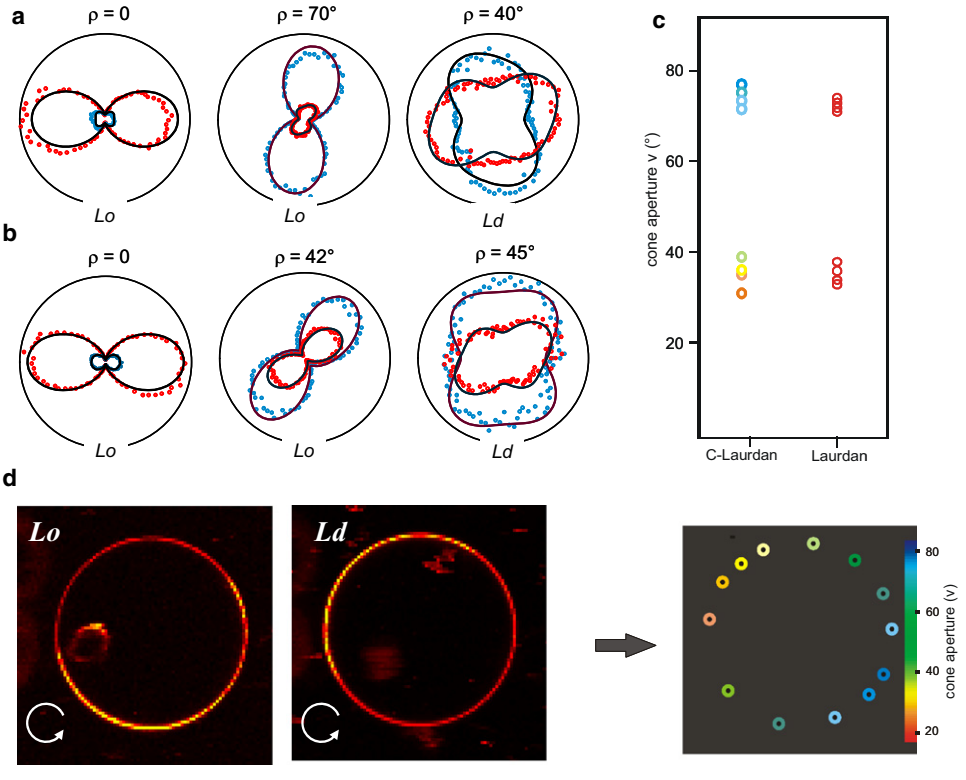


FIGURE 4 Experimental polarimetric responses $I_X$ (*red/dark dots*) and $I_Y$ (*blue/light dots*) of (*a*) C-Laurdan and (*b*) Laurdan, as a function of the input polarization $\alpha$-angle, measured at several locations on the GUVs contour. Spectral detection range: 400–600 nm. The $\rho$-values indicate the distribution orientation obtained from the fit (*continuous lines*) derived from the cone model described in the text. The Lo and Ld phases' assignment is related to the $v$-cone aperture values obtained from the fit. (*c*) Distribution of the angular aperture $v$ obtained from polarimetric measurements performed for each fluorophore. (*d*) Spatial representation of the Lo and Ld phases on a C-Laurdan-labeled GUV, compared to a similar image obtained with spectral filtering (*left*, detection 400 nm ± 20 nm and *right*, detection 560 nm ± 20 nm). TPEF images are obtained at 780-nm excitation with an incident circular polarization to avoid any photoselection effect in the image. The signals from the *X*- and *Y*-sensitive avalanche photodiodes are added to remove the analysis polarization effects. Diameter of the GUV: 50 $\mu$m.

**TABLE 1 Distribution aperture angle $v$ obtained from the polarimetric analysis for the studied molecules in both Lo and Ld lipid phases**

| Phase | C-Laurdan | Laurdan | TMA-DPH | di-8-ANEPPQ |
|---|---|---|---|---|
| Lo | (33 ± 6)° | (36 ± 5)° | (16 ± 4)° | (17 ± 6)° |
| | $\langle P_2\rangle = 1.715$ | $\langle P_2\rangle = 1.674$ | $\langle P_2\rangle = 1.920$ | $\langle P_2\rangle = 1.911$ |
| | $\langle P_4\rangle = 0.415$ | $\langle P_4\rangle = 0.373$ | $\langle P_4\rangle = 0.769$ | $\langle P_4\rangle = 0.745$ |
| | $\langle P_6\rangle = 0.267$ | $\langle P_6\rangle = 0.242$ | $\langle P_6\rangle = 0.602$ | $\langle P_6\rangle = 0.570$ |
| Ld | (73 ± 6)° | (71 ± 4)° | (52 ± 4)° | (46 ± 5)° |
| | $\langle P_2\rangle = 1.320$ | $\langle P_2\rangle = 1.330$ | $\langle P_2\rangle = 1.479$ | $\langle P_2\rangle = 1.546$ |
| | $\langle P_4\rangle = 0.169$ | $\langle P_4\rangle = 0.174$ | $\langle P_4\rangle = 0.241$ | $\langle P_4\rangle = 0.277$ |
| | $\langle P_6\rangle = 0.116$ | $\langle P_6\rangle = 0.119$ | $\langle P_6\rangle = 0.162$ | $\langle P_6\rangle = 0.185$ |

The values are obtained from the measurement of 10 molecules per GUV, measured on five different GUVs in each case. The corresponding order parameters $\langle P_J\rangle$ ($J = 2, 4, 6$) defined in the text are given for the Gaussian distribution shape.

two distinct populations (Fig. 5 *c*) such as previously obtained with Laurdan-type molecules. The spatial location of these populations shows the existence of micrometric size domains, as illustrated on a di-8-ANEPPQ-labeled GUV for which many points have been analyzed along the whole contour (Fig. 5 *d*). Fig. 5 *d* also shows that the di-8-ANEPPQ molecule seems to preferentially locate in the disordered phase, the higher global intensity in this region being a signature of a higher molecular density. Fig. 5 shows finally that the lipid environment local rigidity can be directly probed by an orientational information imaging.

## Determination of $v$ in cell membranes

The orientational behavior of di-8-ANEPPQ molecules was finally investigated in COS-7 cell membranes using the TPEF polarimetry technique. Adherent cells with nonspherical shape were voluntarily chosen to probe the local molecular order in regions where the local orientation of the cell membrane is not easily determined. The equatorial plane of the cells was studied to minimize the effect of the out-of plane angle of the molecular distribution ($\eta$-angle in Fig. 1 *b*). Fig. 6 shows examples together with the data for a few points investigated on the cells contours. In all the investigated cells, the $\rho$-value obtained from the data fitting is roughly consistent with the membrane orientation visible on the cell image. The corresponding $v$-value obtained from the data fitting is found to be larger than for DOPC GUV membranes. This high aperture angle in COS-7 cell membranes has been found reproducibly on several cells over their whole membrane contours.

## Influence the emission/absorption dipoles directions and energy transfer on the polarimetric responses

In addition to the distribution features, two parameters can potentially affect the TPEF polarimetric responses: the angle between the absorption and emission dipoles of the fluorescent probe, and the possible presence of fluorescence resonant energy transfer between neighbor molecules (homo-FRET). Both effects, for which excitation and emission become decorrelated, are expected to introduce a degree of depolarization of the polarization responses, which might lead to a misinterpretation of the polarimetric data. The analysis of these effects is detailed in the Supporting Material.

The dependence of the TPEF signals on the absorption-emission dipoles relative angle $\xi$ (Fig. S4) shows that the polarimetric responses appear to be only slightly dependent on $\xi$ for $\xi < 20°$. By inserting $\xi$ as an additional fitting parameter in the analysis in all the polarimetric responses mentioned above, we have found that

1. the $\xi$-angles for all the studied molecules cannot be higher than 20° (above this angle, the fitting quality is strongly affected), and
2. inserting $\xi$ in the model does not change the resulting angular apertures ($v$, $\rho$) of more than a few percent.

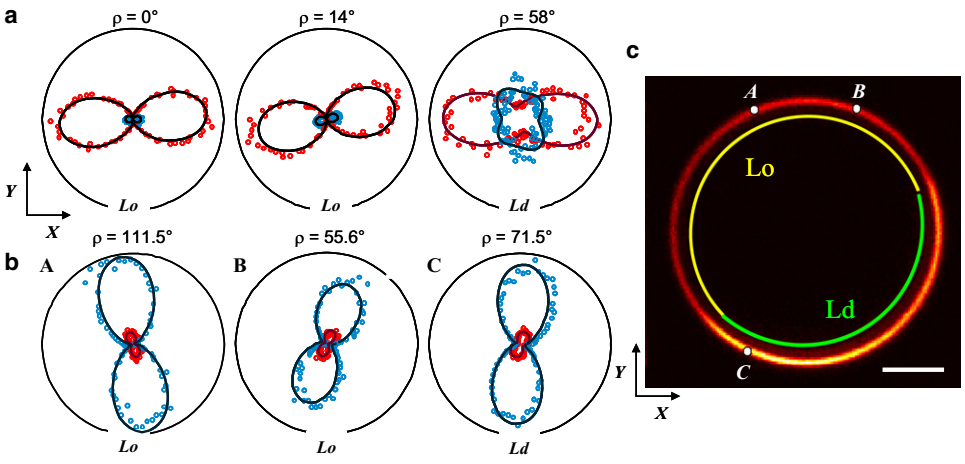


FIGURE 5 Experimental polarimetric responses $I_X$ (*red/dark dots*) and $I_Y$ (*blue/light dots*) emitted by an assembly of (*a*) TMA-DPH and (*b*) di-8-ANEPPQ molecules, measured at several locations on GUV contours. A large spectral band is detected at ~500 nm, with no specific spectral filtering. The indicated $\rho$-values are obtained from the fit (*continuous lines*) derived from the cone model described in the text. The Lo and Ld phases' assignment is related to the $v$-cone aperture values obtained from the fit. (*c*) Distribution of the angular aperture $v$ obtained from polarimetric measurements performed for each fluorophore. (*c*) is the TPEF image of a di-8-ANEPPQ-labeled GUV for a circular input polarization. GUV size: 17 $\mu$m. The color lines superimposed illustrate the spatial location of the Lo and Ld phases deduced from the following $v$-values: $v < 37°$ (Lo) and $v > 37°$ (Ld). Represented points: *A*, $v = 27.8°$; *B*, $v = 12.3°$; and *C*, $v = 46.5°$.

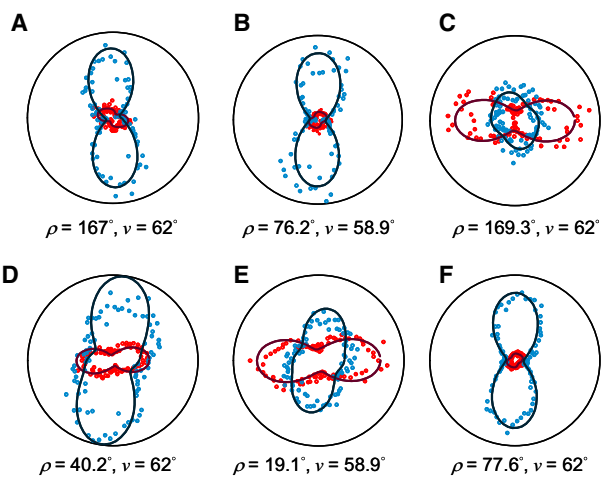


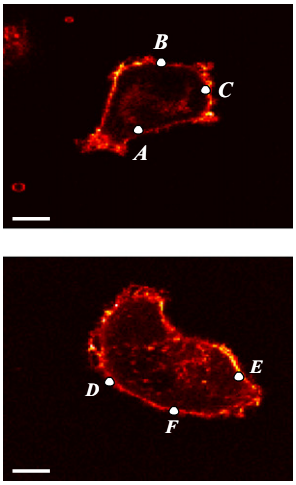


FIGURE 6 Experimental polarimetric responses $I_X$ (*red/dark dots*) and $I_Y$ (*blue/light dots*) from di-8-ANEPPQ molecules labeling COS-7 cells membranes, measured at several locations (indicated by *A–F*) on two different cells contours. The indicated $\rho$- and $\nu$-values are obtained from the fit (*continuous lines*) from the cone model described in the text. Scale bars: 10 $\mu$m.

The found $\xi$ angles are furthermore consistent with the previously published values: $\xi = 19°$ in Prodan (6-propionyl-2-dimethylaminonaphthalene), a molecule similar to the Laurdan and C-Laurdan structures (33), with $\xi = 7–16°$ in TMA-DPH (34).

The sensibility of the TPEF polarimetric responses to the presence of homo-FRET between the molecules in a membrane is analyzed in Fig. S6 using models previously developed (35). The dependence of the polarimetric responses as a function of the energy transfer efficiency shows that above a 10% FRET efficiency, the depolarization effect tends to deform the polarimetric curves, especially at large cone apertures $\nu$. High FRET efficiencies induce a total depolarization illustrated by almost-identical $I_X$ and $I_Y$ polarization dependencies. Introducing homo-FRET in the analysis of the polarimetric experimental data in GUVs and cells tends to slightly improve the quality of the fit of both $I_X$ and $I_Y$ polarization dependence; however, the final values obtained for both $\nu$- and $\rho$-parameters do not change significantly. This shows, in particular, that the homo-FRET efficiency in the system is low (<10%). This is consistent with the distance between fluorescent molecules (estimated to ~10 nm accounting for their dilution and a typical lipid cross section of ~50 Å), which is larger than the typical distances (a few nanometers) over which a 50% FRET efficiency occurs.

## DISCUSSION

The TPEF polarimetric imaging technique, based on a tunable incident polarization and a polarized readout, is shown to be able to provide information on the molecular angular distribution in different lipid environments at any place of GUV and cell membranes, whatever their local curvature.

To compare this technique with the more traditional fluorescence anisotropy, we define the polarization factor ratio $A = (I_Y - I_X)/(I_Y + I_X)$ measured for a circular incident excitation. $A$ varies between (+1) when the fluorescence dipoles lye along $Y$ ($\rho = \pi/2$), and (−1) when they lie along the $X$ direction ($\rho = 0$). All intermediate values will be reached if the molecular orientations are either distributed within a cone (of aperture $\nu$), or globally rotated (of an angle $\rho$). An image of the $A$ factor is depicted in Fig. 7 *a* for a DOPC GUV doped with C-Laurdan (similar images have been obtained for the other studied fluorescent probes). Interpreting such an image first requires the knowledge of the mean orientation of the molecules relative to the membrane-normal direction. The $A(\rho,\nu)$ function (Fig. 7 *c*) can be used to determine $\nu$, assuming a known cone mean orientation $\rho$, as used in previous works (4,5), where the membrane-normal or tangential directions were assumed to coincide with the mean molecular orientation. The anisotropy image is more

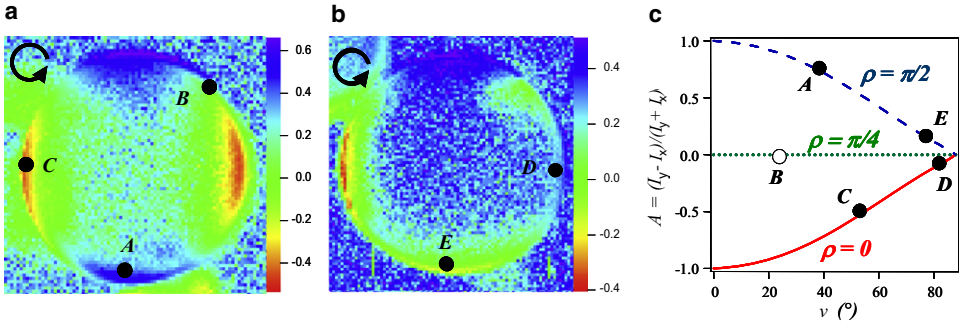


FIGURE 7 Images of the polarization factor ratio $A$ defined in the text, of C-Laurdan-labeled GUV formed by (*a*) DOPC and (*b*) DOPC/Chol/SM (1:1:1). (*c*) $A$ factor calculated for a cone aperture model, at different cone mean orientations: $\rho = 90°$(*dashed line*), $\rho = 45°$(*dotted line*), $\rho = 0°$(*solid line*). Measured points are indicated by *A–E*.

complex in the case of lipid mixtures, as illustrated for C-Laurdan in a DOPC/Chol/SM GUV (Fig. 7 *b*). Fig. 7, *a* and *b*, can be analyzed assuming that the cone orientation and membrane normal direction coincide. As readily seen for C-Laurdan in a DOPC GUV (Fig. 7 *a*), anisotropy values at points *A* and *C* in Fig. 7 *c* do not surpass $A \pm 0.4$, for which $v = 60°–80°$. In a GUV formed by a (DOPC/Chol/SM) lipid mixture (Fig. 7 *b*), the *v* parameter varies roughly from 30° to 80° (points *D* and *E* in Fig. 7 *b* are most probably in disordered regions). These values are of same order of magnitude as the ones found from the TPEF polarimetric measurements described above. Measurement points at $\sim\rho = \pi/4$ (point *B*) are not exploitable, as *A* is insensitive to the molecular order in this case (Fig. 7 *c*). Therefore with this pure anisotropy measurement, it is not possible to distinguish the complete spatial localization of Lo and Ld phases.

As the TPEF polarimetric measurements developed in this work does not require the knowledge of the molecules mean orientation, it has been applied directly to random positions taken on GUVs or nonspherical cells. Different parameters (nature of the angular distribution, excitation-emission dipole angle, homo-FRET) have been computed and taken into account for the estimation of the *v*-angle in Lo-Ld two-phase GUVs and COS-7 cells.

Measurements performed on GUVs show that molecular order is strongly dependent on the fluorescent probe structure, primarily because it is driven by lipid-fluorophore interactions that are influenced by the molecular head position. Cone aperture values obtained for both C-Laurdan and Laurdan show that their orientational behavior deviates substantially from a perfect orientational order. In the Ld phase, where the lipid acyl chains are highly disordered, the aperture angle is significantly increased. The reason for the relatively high disorder in both Lo and Ld phases might occur from the fact that these molecules locate in the hydrophobic part of the membrane due to van der Waals interaction between their Lauric chains and the lipid chains (27,36), as also observed in DPH-derivative fluorophores embedded in the membrane (5). Although C-Laurdan seems to explore a larger range of cone apertures than other fluorophores (Fig. 4 *d*), superimposing aperture angles and lipid phase images also shows a large spatial variation between ordered and disordered regions. In particular, C-Laurdan is overall seen to be a more sensitive probe of local orientational order, as also observed in previous works (27).

In the case of TMA-DPH and di-8-ANEPPQ, although the Lo or Ld environment cannot be identified from a control spectral measurement, the TPEF polarimetric analysis permitted us to directly create an image of the spatial distribution of molecular order (Fig. 5 *d*). The cone aperture values obtained are globally lower than for the Laurdan type molecules, which is consistent with their inclusion localization in the periphery part of the membrane. TMA-DPH, located near the more ordered headgroup region, has been reported to exhibit quasi-one-dimensional order in gel phases with cone aperture angles below 20° (2), which is consistent with the values found here in Lo regions. A similar behavior is observed for di-8-ANEPPQ, although with a slightly higher flexibility (Fig. 5 *c*). The values obtained for di-8-ANEPPQ in Ld phases are close to the ones found for the BODIPY-PC fluorescent lipid probe (4).

TPEF polarimetry measurements on COS-7 cells show that the molecules mean orientation roughly lies along the membrane-normal direction. However, in many points the membrane is of complex shape and its global orientation difficult to visualize. The simultaneous fitting on both $\rho$- and *v*-parameters makes it possible to avoid speculating on the local membrane contour as previously done (4,9).

The measured cone aperture angle on COS-7 cell membranes shows that the di-8-ANEPPQ probes behave in a slightly more disordered way than in DOPC GUV membranes. Opposite disorder properties have been previously found when comparing DOPC and cell membranes (29) in a solution of reconstructed vesicles. Possible artifact origins to our observation have been ruled out. First, the number of molecules present in the membrane is too low to provoke homo-FRET effects. Second, the presence of the rather small isotropic contribution of the intracellular partitioning of the fluorescent probe is seen to not affect the measurement, as ascertained by the evolution of the polarimetric data when decreasing the size of the integration area (below a few pixels, close to the diffraction limit, the polarimetric data remain identical). A possible hypothesis of this relatively high degree of disorder is the membrane local morphology. Indeed, a preliminary study shows that, when decreasing the osmotic pressure of the surrounding medium, which makes the cells more spherical, the aperture angle tends to decrease closer to the DOPC GUV values. This measurement seems finally to highlight the properties of the membrane subresolution scale structure: below the 300-nm optical limit, any disorder of the membrane at nanometer scales (ruffling, vesiculation) will lead to an increase of the measured cone aperture of the probe molecules. In a more general context, TPEF polarimetry can be applied to the imaging of heterogeneous membranes organization occurring in endocytosis, exocytosis (3), and cell surface ruffling (9).

## CONCLUSION

The sensitivity of polarimetric TPEF allows the identification of quantitative features of the molecular angular distribution in membranes. The spatial identification of molecular order behaviors in heterogeneous lipid and cell membranes can be used as a new type of probe of the lipid environment. This possibility opens the scope of structural studies to complex geometries of cells and biomolecular assemblies of a priori unknown nature.

## SUPPORTING MATERIAL

Six figures are available at http://www.biophysj.org/biophysj/supplemental/S0006-3495(09)01442-8.

We thank Patrick Ferrand for support in the polarimetric microscopy setup development. We thank Didier Marguet and Hai Tao He from Centre d'Immunology de Marseille Luminy, France, for fruitful discussions.

This work was supported by the French Agence Nationale de la Recherche under program No. JC 2007 (project NLO-Shaping grant No. JC07-195504), the European Commission through the Human Potential Program Marie-Curie RTN NANOMATCH (grant No. MRTN-CT-2006-035884), and the Korea Science and Engineering Foundation grant (No. R0A-2007-000-20027-0) funded by the Korea Ministry of Education, Science, and Technology.

## REFERENCES

1. Axelrod, D. 1979. Carbocyanine dye orientation in red cell membrane studied by microscopic fluorescence polarization. *Biophys. J.* 26: 557–573.
2. Florine-Casteel, K. 1990. Phospholipid order in gel- and fluid-phase cell-size liposomes measured by digitized video fluorescence polarization microscopy. *Biophys. J.* 57:1199–1215.
3. Sund, S. E., J. A. Swanson, and D. Axelrod. 1999. Cell membrane orientation visualized by polarized total internal reflection fluorescence. *Biophys. J.* 77:2266–2283.
4. Benninger, R. K., M. A. Neil, D. M. Davis, and P. M. French. 2005. Fluorescence imaging of two-photon linear dichroism: cholesterol depletion disrupts molecular orientation in cell membranes. *Biophys. J.* 88:609–622.
5. Haluska, C. K., A. P. Schröder, P. Didier, D. Heissler, G. Duportail, et al. 2008. Combining fluorescence lifetime and polarization microscopy to discriminate phase-separated domains in giant unilamellar vesicles. *Biophys. J.* 95:5737–5747.
6. Borejdo, J., and S. Burlacu. 1993. Measuring orientation of actin filaments within a cell: orientation of actin in intestinal microvilli. *Biophys. J.* 65:300–309.
7. Rocheleau, J. V., M. Edidin, and D. W. Piston. 2003. Intrasequence GFP in Class I MHC molecules, a rigid probe for fluorescence anisotropy measurements of the membrane environment. *Biophys. J.* 84:4078–4086.
8. Vrabioiu, A. M., and T. J. Mitchison. 2006. Structural insights into yeast septin organization from polarized fluorescence microscopy. *Nature.* 443:466–468.
9. Benninger, R. K. P., B. Vanherberghen, S. Young, S. B. Taner, F. J. Culley, et al. 2009. Live cell linear dichroism imaging reveals extensive membrane ruffling within the docking structure of natural killer cell immune synapses. *Biophys. J.* 96:L13–L15.
10. Dale, R., S. C. Hopkins, U. A. an der Heide, T. Marszalek, M. Irving, et al. 1999. Model-independent analysis of the orientation of fluorescent probes with restricted mobility in muscle fibers. *Biophys. J.* 78:1606–1618.
11. LeFloc'h, V. 2003. Monitoring of orientation in molecular ensembles by polarization sensitive nonlinear microscopy. *J. Phys. Chem. B.* 107:12403–12410.
12. Anceau, C., S. Brasselet, and J. Zyss. 2005. Local orientational distribution of molecular monolayers probed by nonlinear microscopy. *Chem. Phys. Lett.* 411:98–102.
13. Brasselet, S., V. LeFloc'h, F. Treussart, J. Roch, J. Zyss, et al. 2004. In situ diagnostics of the crystalline nature of single organic nanocrystals by nonlinear microscopy. *Phys. Rev. Lett.* 92:207401.
14. Brasselet, S., and J. Zyss. 2007. Nonlinear polarimetry of molecular crystals down to the nanoscale. *C. R. Phys.* 8:165–179.
15. Dietrich, C., L. A. Bagatolli, Z. N. Volovyk, N. L. Thompson, M. Levi, et al. 2001. Lipid rafts reconstituted in model membranes. *Biophys. J.* 80:1417–1428.
16. Samsonov, A. V., I. Mihalyov, and F. S. Cohen. 2001. Characterization of cholesterol-sphingomyelin domains and their dynamics in bilayer membranes. *Biophys. J.* 81:1486–1500.
17. Scherfeld, D., N. Kahya, and P. Schwille. 2003. Lipid dynamics and domain formation in model membranes composed of ternary mixtures of unsaturated and saturated phosphatidylcholines and cholesterol. *Biophys. J.* 85:3758–3768.
18. Baumgart, T., S. T. Hess, and W. W. Webb. 2003. Imaging coexisting fluid domains in biomembrane models coupling curvature and line tension. *Nature.* 425:821–824.
19. Simons, K., and E. Ikonen. 1997. Functional rafts in cell membranes. *Nature.* 387:569–572.
20. Ikonen, E. 2001. Roles of lipid rafts in membrane transport. *Curr. Opin. Cell Biol.* 13:470–477.
21. Veatch, S. L., and S. L. Keller. 2002. Organization in lipid membranes containing cholesterol. *Phys. Rev. Lett.* 89:268101.
22. Kahya, N., D. Scherfeld, K. Bacia, B. Poolman, and P. Schwille. 2003. Probing lipid mobility of raft-exhibiting model membranes by fluorescence correlation spectroscopy. *J. Biol. Chem.* 278:28109–28115.
23. McConnell, H. M., and M. Vrljic. 2003. Liquid-liquid immiscibility in membranes. *Annu. Rev. Biophys. Biomol. Struct.* 32:469–492.
24. Edidin, M. 2003. The state of lipid rafts: from model membranes to cells. *Annu. Rev. Biophys. Biomol. Struct.* 32:257–283.
25. Munro, S. 2003. Lipid rafts: elusive or illusive? *Cell.* 115:377–388.
26. Bagatolli, L. A., and E. Gratton. 1999. Two-photon fluorescence microscopy observation of shape changes at the phase transition in phospholipid giant unilamellar vesicles. *Biophys. J.* 77:2090–2101.
27. Kim, H. M., H.-J. Choo, S.-Y. Jung, Y.-G. Ko, W.-H. Park, et al. 2007. A two-photon fluorescent probe for lipid raft imaging: C-Laurdan. *ChemBioChem.* 8:553–559.
28. Baumgart, T., G. Hunt, E. R. Farkas, W. W. Webb, and G. W. Feigenson. 2007. Fluorescence probe partitioning between Lo/Ld phases in lipid membranes. *Biochim. Biophys. Acta.* 1768:2182–2194.
29. Gidwani, A., D. Holowka, and B. Baird. 2001. Fluorescence anisotropy measurements of lipid order in plasma membranes and lipid rafts from RBL-2H3 mast cells. *Biochemistry.* 40:12422–12429.
30. Angelova, M. I., and D. S. Dimitrov. 1986. Liposome electroformation. *Faraday Discuss. Chem. Soc.* 81:303–311.
31. Kinosita, K., S. Kawato, and A. Ikegami. 1977. A theory of fluorescence polarization decay in membranes. *Biophys. J.* 20:289–305.
32. Schön, P., F. Munhoz, A. Gasecka, S. Brustlein, and S. Brasselet. 2008. Polarization distortion effects in polarimetric two-photon microscopy. *Opt. Express.* 16:20891–20901.
33. Moyano, F., M. A. Biasutti, J. J. Silber, and N. M. Correa. 2006. New insights on the behavior of Prodan in homogeneous media and in large unilamellar vesicles. *J. Phys. Chem. B.* 110:11838–11846.
34. Muller, J. M., D. H. Harryvan, J. C. D. Verhagen, E. E. v. F, and G. van Ginkel. 1996. The orientation of the transition dipole moments of TMA-DPH embedded in a poly(vinyl alcohol) film. *Chem. Phys.* 211:413–420.
35. Clegg, R. M. 1996. Fluorescence imaging spectroscopy and microscopy: fluorescence resonance energy transfer. *In* Chemical Analysis, *Vol. 137*, 13th Ed. Wiley, New York.
36. Chong, P. L. G., and P. T. T. Wong. 1993. Interactions of Laurdan with phosphatidylcholine liposomes: a high pressure FTIR study. *Biochim. Biophys. Acta.* 1149:260–266.